

From complex magnetism ordering to simple ferromagnetism in two-dimensional LaCrSb₃ by hole doping

Haijie Chen,^{1,3} Awadhesh Narayan,⁴ Lei Fang,^{1,3} Nicholas P. Calta,¹ Fengyuan Shi,² Duck Young Chung,³ Lucas K. Wagner,⁴ Wai-Kwong Kwok,³ and Mercouri G. Kanatzidis^{1,2,3,*}

¹Department of Chemistry, Northwestern University, Evanston, Illinois 60208, USA

²Department of Materials Science and Engineering, Northwestern University, Evanston, Illinois 60208, USA

³Materials Science Division, Argonne National Laboratory, Argonne, Illinois 60439, USA

⁴Department of Physics, University of Illinois at Urbana-Champaign, Illinois 61801, USA

(Received 8 June 2016; revised manuscript received 18 August 2016; published 11 October 2016)

Competing orders widely exist in many material systems, such as superconductivity, magnetism, and ferroelectricity; LaCrSb₃ is a highly anisotropic magnetic material in which the spins are aligned ferromagnetically in one direction and canted antiferromagnetically in another in the Cr-Sb chains. Hole doping with Sr²⁺ and Ca²⁺ in the La site suppresses the antiferromagnetic correlations and transforms the anisotropic magnetic order into a ferromagnetic lattice in all directions. First-principles density functional theory calculations show that the canted magnetic order becomes energetically less favorable compared to the FM order upon hole doping. Doping in the La site is an effective approach to modulate the competing orders in LaCrSb₃.

DOI: [10.1103/PhysRevB.94.134411](https://doi.org/10.1103/PhysRevB.94.134411)

I. INTRODUCTION

Materials with competing orders are of broad interest because they can lead to novel physical phenomena, such as high temperature superconductivity [1–3], colossal magnetoresistance [4], and ferroelectricity [5–7]. Tuning and controlling competing orders are of high importance for understanding materials properties, as well as for potential applications. For example, in the iron-based pnictides, both spin density wave and superconductivity exist in the phase diagram [3,8–10], antiferromagnetic (AFM) fluctuations are associated with superconductivity in heavy fermion compounds [2,11–13], and the ferromagnetic (FM) and AFM configurations compete in colossal magnetoresistance systems [4,14,15]. Often, these situations occur in materials with low dimensional structures.

To explore the presence of FM and AFM competing orders, we focused on LaCrSb₃ because of its two-dimensional structure, unusual magnetic coupling behavior of the Cr atoms, and the presence of a flat perfect square net of Sb atoms in the structure, the latter of which may be a source of density wave behavior [16–23]. RECrSb₃ (RE = rare-earth metals), a series of ternary intermetallic rare earth chromium antimonides, have rich and perplexing magnetic orderings [24–30]. An archetypal compound of the RECrSb₃ series, LaCrSb₃ has a rich magnetic phase diagram and relative simplicity in magnetic nature due to the absence of 4*f* electrons in La³⁺ [31–35]. Below ~95 K, the spins are ordered ferromagnetically in the *b* direction and canted antiferromagnetically in the *c* direction [34]. Previous studies have suggested that the AFM configuration has an itinerant nature [31,33], while more detailed studies show that the localized Cr spins also contributes to the magnetic behavior [34]. Partial substitution of Cr by other elements suppresses the AFM long range order [32,35]. However, the FM order is also suppressed as a result of doping in the Cr site. Doping with other magnetic rare-earth elements in the La site has shown an even more complicated magnetic phase diagram [29].

In LaCrSb₃, we aim to induce a substantial lowering of the Fermi energy to investigate the effects of magnetic coupling on Cr to probe for competing states. Our approach focuses on doping the La atom sublattice with aliovalent elements (such as Sr²⁺ and Ca²⁺) to achieve “oxidation” on the Cr-Sb chain structure. Doping the La site with alkaline earth 2+ ions does not cause substitutional disorder on the magnetic Cr sublattice nor on the square net Sb sublattice. Instead of combined FM and AFM orders, a simple FM lattice is observed. Our density functional theory (DFT) calculations are in qualitative agreement with our experimental findings, and show that the canted magnetic order becomes energetically less favorable compared to FM order upon hole doping.

II. RESULTS AND DISCUSSION

A. Synthesis and structure

The structure of LaCrSb₃, as shown in Fig. 1(a), consists of Cr-Sb layers and Sb square nets separated by La³⁺ cations along the *a* axis. The Cr-Sb layer is formed by face-sharing CrSb₆ octahedra and extended along the *bc* plane. Figure 1(b) shows the spin canting in pristine LaCrSb₃ that leads to the emergence of an AFM order <95 K [34]. The canted spin arrangement generates opposite spin polarity in the *c* axis, forming an AFM exchange interaction.

To successfully introduce Sr or Ca in the structure of LaCrSb₃, a large excess of alkaline earth metals was used. The molar ratio of [Sr, Ca] to La needs to be greater than one. However, when the [Sr, Ca]/La molar ratio was >2.5, no single crystals were obtained. Below this ratio, the obtained single crystals were pure LaCrSb₃ (see Fig. S1 in the Supplemental Material [36]). For higher dopant concentrations, both Ca²⁺ and Sr²⁺ successfully dope LaCrSb₃ on the La site, as confirmed by energy dispersive x-ray spectroscopy and scanning electron microscopy (EDS/SEM; Figs. S2 and S3 [36]). For the Sr²⁺ doped crystals, the actual doping level *x* was found to vary from 0.05 to 0.15 and for the Ca²⁺ doped crystals, between 0.15 and 0.60. The platelike single crystals display shiny metallic

*Corresponding author: m-kanatzidis@northwestern.edu

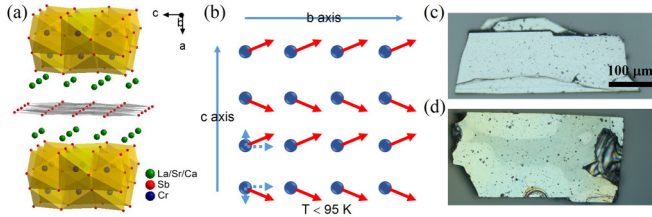


FIG. 1. (a) Crystal structure of LaCrSb₃ as viewed along the *b* axis. The La (Sr, Ca), Cr, and Sb atoms are shown as green, blue, and red spheres, respectively. The planar Sb square net is labeled grey. (b) Projection of the Cr sublattice onto the *bc* plane. The arrows represent the Cr magnetic structures below 95 K [34]. Typical images of (c) LaCrSb₃ and (d) Ca doped LaCrSb₃ single crystals with smooth surface.

color with typical dimensions of $\sim 0.1 \text{ mm} \times 0.5 \text{ mm} \times 0.02 \text{ mm}$ [Figs. 1(c) and 1(d)].

For accuracy, single-crystal structures of La_{1-x}Sr_xCrSb₃ and La_{1-x}Ca_xCrSb₃ were determined using x-ray diffraction at room temperature (293 K). The crystallographic data and

structural refinements for samples with the highest doping level are listed in Table I. The results for samples with other doping levels are listed in Tables S1–S4 in the Supplemental Material [36]. All of the compounds crystallize in the same orthorhombic space group *Pbcm*. For LaCrSb₃, the unit cell parameters are $a = 13.274(3) \text{ \AA}$, $b = 6.2028(12) \text{ \AA}$, and $c = 6.1086(12) \text{ \AA}$, which are slightly smaller than previously reported data ($a = 13.2835(7) \text{ \AA}$, $b = 6.2127(2) \text{ \AA}$, and $c = 6.116(1) \text{ \AA}$) [24]. Fractional atomic coordinates and thermal displacement parameters (U_{eq}) for La_{1-x}Sr_xCrSb₃ and La_{1-x}Ca_xCrSb₃ are listed in Tables S5 and S6, respectively [36]. Anisotropic displacement parameters are presented in Tables S7 and S8 [36].

For La_{1-x}Sr_xCrSb₃, refined x-ray diffraction gives $x = 0, 0.05(8), 0.08(3)$, and $0.16(3)$, in agreement with the EDS/SEM results. The determined lattice parameters increase with higher doping levels generating larger cell volumes, consistent with the introduction of the larger Sr²⁺ ion into the La site in LaCrSb₃. The higher doping level for La_{1-x}Ca_xCrSb₃ with $x = 0.14(1), 0.31(3)$, and $0.62(3)$ indicates that the smaller Ca²⁺ ion substitutes La³⁺ more easily in the LaCrSb₃ system.

TABLE I. Crystal data and structure refinements for LaCrSb₃, La_{0.83(7)}Sr_{0.16(3)}CrSb₃, and La_{0.37(7)}Ca_{0.62(3)}CrSb₃.^a

Empirical formula, <i>Z</i>	LaCrSb ₃ , 4	La _{0.83(7)} Sr _{0.16(3)} CrSb ₃ , 4	La _{0.37(7)} Ca _{0.62(3)} CrSb ₃ , 4
Formula weight	556.16	547.83	494.64
Crystal system		Orthorhombic	
Space group		<i>Pbcm</i>	
<i>a</i> (Å)	13.274(3)	13.336(3)	13.282(3)
<i>b</i> (Å)	6.2028(12)	6.2029(12)	6.1740(12)
<i>c</i> (Å)	6.1086(12)	6.1120(12)	6.0506(12)
Volume (Å ³)	502.97(17)	505.61(17)	496.18(17)
Calculated density (g/cm ³)	7.345	7.197	6.622
Absorption coefficient (mm ⁻¹)	26.117	26.340	21.903
<i>F</i> (000)	936	924	844
Crystal size (mm ³)	0.1080 × 0.0701 × 0.0202	0.0946 × 0.0483 × 0.0035	0.2114 × 0.1019 × 0.0239
θ range for data collection (deg)	3.07 to 29.13	1.53 to 29.14	3.07 to 29.19
Index ranges	$-18 \leq h \leq 18$ $-8 \leq k \leq 8$ $-8 \leq l \leq 8$	$-18 \leq h \leq 18$ $-8 \leq k \leq 8$ $-8 \leq l \leq 8$	$-17 \leq h \leq 18$ $-8 \leq k \leq 8$ $-8 \leq l \leq 8$
Reflections collected	4590	4572	4521
Independent reflections	740 [$R_{int} = 0.0629$]	746 [$R_{int} = 0.0452$]	737 [$R_{int} = 0.0612$]
Completeness	99.7% to $\theta = 29.13^\circ$	99.9% to $\theta = 29.14^\circ$	99.9% to $\theta = 29.19^\circ$
Refinement method		Full matrix least squares on F^2	
Data/restraints/parameters	740/0/30	746/0/31	737/0/31
Goodness of fit	1.155	1.149	1.176
Final <i>R</i> indices [$> 2\sigma(I)$] ^b	$R_{obs} = 0.0326$, $wR_{obs} = 0.0725$	$R_{obs} = 0.0279$, $wR_{obs} = 0.0608$	$R_{obs} = 0.0360$, $wR_{obs} = 0.0763$
<i>R</i> indices [all data] ^b	$R_{all} = 0.0406$, $wR_{all} = 0.0749$	$R_{all} = 0.0365$, $wR_{all} = 0.0632$	$R_{all} = 0.0457$, $wR_{all} = 0.0789$
Extinction coefficient	0.0150(7)	0.0036(3)	0.0019(3)
Largest diffraction peak and hole ($e \cdot \text{\AA}^{-3}$)	1.741 and -3.329	2.856 and -2.547	1.513 and -2.232

^aFor all structures, $T = 293(2) \text{ K}$ and $\lambda = 0.71073 \text{ \AA}$.

^b $R = \sum ||F_o| - |F_c|| / \sum |F_o|$, $wR = \{ \sum [w(|F_o|^2 - |F_c|^2)^2] / \sum [w(|F_o|^4)] \}^{1/2}$ and $w = 1 / [\sigma^2(F_o^2) + (A \times P)^2 + (B \times P)]$, where $P = (F_o^2 + 2F_c^2) / 3$. For LaCrSb₃, $A = 0.0434$ and $B = 0.0000$. For La_{0.83(7)}Sr_{0.16(3)}CrSb₃, $A = 0.0370$ and $B = 0.0000$. For La_{0.37(7)}Ca_{0.62(3)}CrSb₃, $A = 0.0345$ and $B = 3.6017$.

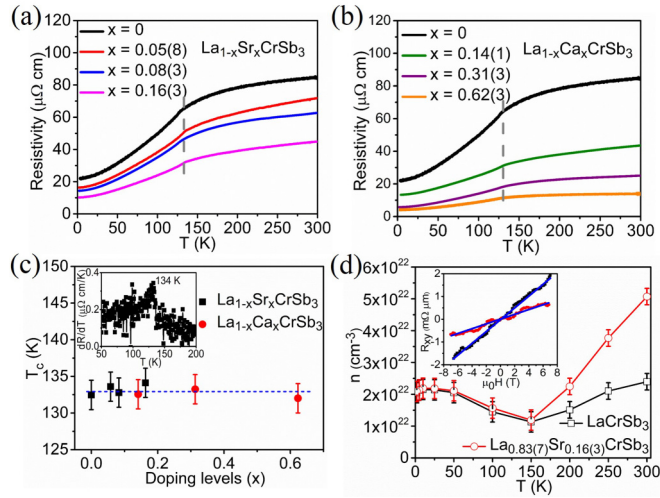


FIG. 2. Temperature-dependent resistivity along the c axis for (a) $\text{La}_{1-x}\text{Sr}_x\text{CrSb}_3$ ($x = 0, 0.05(8), 0.08(3), 0.16(3)$) and (b) $\text{La}_{1-x}\text{Ca}_x\text{CrSb}_3$ ($x = 0, 0.14(1), 0.31(3), 0.62(3)$), respectively. (c) The determined Curie temperature (T_c) versus doping levels (x). Inset: determined T_c in $\text{La}_{0.83(7)}\text{Sr}_{0.16(3)}\text{CrSb}_3$ by temperature-dependent dR/dT . (d) Temperature-dependent carrier density (n). The inset is the room temperature Hall resistivity at 300 K that displays linear field dependence.

B. Charge transport

The electrical resistivity of $\text{La}_{1-x}\text{Sr}_x\text{CrSb}_3$ ($x = 0, 0.05(8), 0.08(3), 0.16(3)$) and $\text{La}_{1-x}\text{Ca}_x\text{CrSb}_3$ ($x = 0, 0.14(1), 0.31(3), 0.62(3)$), as measured along the c axis of single crystal samples, are shown in Figs. 2(a) and 2(b), respectively. The electrical resistivity decreases upon cooling for all measured samples, indicative of metallic behavior. The introduction of Sr^{2+} and Ca^{2+} decreases the resistivity. For $\text{La}_{1-x}\text{Sr}_x\text{CrSb}_3$ ($x = 0, 0.05(8), 0.08(3), 0.16(3)$) and $\text{La}_{1-x}\text{Ca}_x\text{CrSb}_3$ ($x = 0, 0.14(1), 0.31(3), 0.62(3)$), the resistivity decreases from 85 to $45\mu\Omega\text{ cm}$ and from 85 to $14\mu\Omega\text{ cm}$, respectively. All of the data show a slight drop at around 130 K, which may be due to reduced electron-spin scattering below the ferromagnetic transition [33]. As plotted in Fig. 2 (c), the introduction of neither Sr^{2+} nor Ca^{2+} causes the anomaly to shift, indicating that the Curie temperature (T_c) is almost identical for all samples. The magnetic transition in undoped LaCrSb_3 is due to the Cr 3d electrons [33]. Considering that Cr^{3+} is the only magnetic ion in this system, it is reasonable that the doping of the La site with some Sr^{2+} and Ca^{2+} does not change the T_c . As displayed in Figs. S4 and S5 in the Supplemental Material [36], the resistivity decreases linearly with T above the transition temperature and as $T^{3/2}$ below it, which is typical for FM systems [36,37].

The Hall effect was measured to probe the conducting carriers. Considering that both Sr^{2+} and Ca^{2+} are expected to act as acceptors and induce hole doping, we investigated two samples, LaCrSb_3 and $\text{La}_{0.83(7)}\text{Sr}_{0.16(3)}\text{CrSb}_3$. The Hall resistivity $R_{xy} = [R(+H) - R(-H)]/2$ was obtained by switching the magnetic field at each point to reduce the effect of Hall electrode misalignment. R_{xy} versus magnetic field $\mu_0 H$ at different temperatures for LaCrSb_3 and $\text{La}_{0.83(7)}\text{Sr}_{0.16(3)}\text{CrSb}_3$ are shown in Figs. S6 and S7, respec-

tively, in the Supplemental Material [36]. The calculated temperature-dependent carrier density (n) is presented in Fig. 2(d). The inset shows the linear field dependence of the Hall resistivity at 300 K. The positive R_{xy} indicates that the dominant charge carriers are holes in both LaCrSb_3 and $\text{La}_{0.83(7)}\text{Sr}_{0.16(3)}\text{CrSb}_3$ as expected; R_{xy} decreases linearly with decreasing magnetic field. The temperature-dependent variance in both samples shows similar behavior. For LaCrSb_3 , the hole carrier concentration n ($\sim 2.4 \times 10^{22}\text{ cm}^{-3}$) decreases with decreasing temperature until $T = 150\text{ K}$ ($\sim 1.1 \times 10^{22}\text{ cm}^{-3}$). Below 150 K, n increases as the temperature decreases further ($\sim 2.1 \times 10^{22}\text{ cm}^{-3}$ at 5 K). For $\text{La}_{0.83(7)}\text{Sr}_{0.16(3)}\text{CrSb}_3$, n varies as $\sim 5.1 \times 10^{22}\text{ cm}^{-3}$ at 300 K, $\sim 1.1 \times 10^{22}\text{ cm}^{-3}$ at 150 K, and $\sim 2.1 \times 10^{22}\text{ cm}^{-3}$ at 5 K. The increased carrier concentration for the hole doped $\text{La}_{0.83(7)}\text{Sr}_{0.16(3)}\text{CrSb}_3$ confirms the hole doping and the resultant decrease of the resistivity. Earlier studies on charge transport properties of LaCrSb_3 also reported its hole-type behavior, which could be attributed to double-exchange interaction in the Cr-Sb chains [34,38]. The calculated mobility at 300 K of doped $\text{La}_{0.83(7)}\text{Sr}_{0.16(3)}\text{CrSb}_3$ is $\sim 2.7\text{ cm}^2\text{ V}^{-1}\text{ s}^{-1}$ which is slightly smaller than that of LaCrSb_3 ($\sim 3.1\text{ cm}^2\text{ V}^{-1}\text{ s}^{-1}$). The introduction of dopants in the La site seems to have a minor effect on the mobility.

C. Magnetization

The magnetization as a function of field (0–2 T) at 5 K along the a , b , and c axes for LaCrSb_3 , $\text{La}_{0.83(7)}\text{Sr}_{0.16(3)}\text{CrSb}_3$, and $\text{La}_{0.37(7)}\text{Ca}_{0.62(3)}\text{CrSb}_3$ are shown in Figs. 3(a)–3(c), respectively. Further magnetization at a small magnetic field (0–5 kOe) is shown in Fig. S8 in the Supplemental Material [36]. The magnetization shows highly anisotropic behavior along the different directions. In all three compounds, the magnetization along the b axis saturates almost immediately with applied field. The magnetization along the c axis saturates at higher fields to magnetization values close to that of the b axis. In contrast, the magnetization along the a axis increases linearly with increasing field with no evidence of saturation. The magnetization behavior along the b and a axes for the Sr^{2+} and Ca^{2+} doped samples is similar to that of pristine LaCrSb_3 . For the data along the c axis, the bump present in LaCrSb_3 at around 0.2 T, which is due to the AFM ordering along the c axis [33], disappears in the doped samples. This implies that in the doped samples the AFM order is suppressed.

The 1000 Oe field-cooled (FC) magnetization versus temperature curves (M - T) along the a , b , and c axes for LaCrSb_3 , $\text{La}_{0.83(7)}\text{Sr}_{0.16(3)}\text{CrSb}_3$, and $\text{La}_{0.37(7)}\text{Ca}_{0.62(3)}\text{CrSb}_3$ is shown in Figs. 3(d)–3(f), respectively. It is clear that the AFM order in LaCrSb_3 is suppressed as a result of Sr^{2+} or Ca^{2+} doping, and the system transforms into a pure FM material, which is further confirmed by the 10 Oe FC M - T results in Fig. S8 in the Supplemental Material [36]. Figures S9 and S10 summarize the temperature dependence magnetization for all samples with different doping levels along the b axis [36]. The introduction of Sr^{2+} and Ca^{2+} leads to a minor increased moment. For LaCrSb_3 , the magnetization along the b axis at 5 K is $1.19\mu_B/\text{f.u.}$. For $\text{La}_{0.83(7)}\text{Sr}_{0.16(3)}\text{CrSb}_3$ and $\text{La}_{0.37(7)}\text{Ca}_{0.62(3)}\text{CrSb}_3$, this value increases to $1.39\mu_B/\text{f.u.}$ and $1.58\mu_B/\text{f.u.}$, respectively. The FM transition temperature

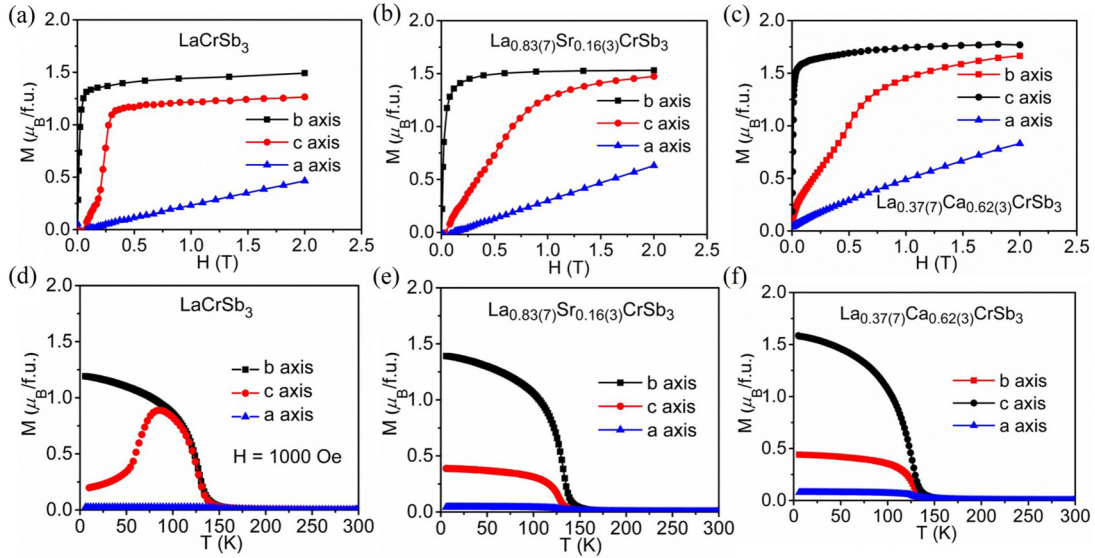


FIG. 3. Magnetization as a function of magnetic field at 5 K along the b (black), c (red), and a (blue) axes for (a) LaCrSb_3 , (b) $\text{La}_{0.83(7)}\text{Sr}_{0.16(3)}\text{CrSb}_3$, and (c) $\text{La}_{0.37(7)}\text{Ca}_{0.62(3)}\text{CrSb}_3$. Temperature dependence of magnetization for (d) LaCrSb_3 , (e) $\text{La}_{0.83(7)}\text{Sr}_{0.16(3)}\text{CrSb}_3$, and (f) $\text{La}_{0.37(7)}\text{Ca}_{0.62(3)}\text{CrSb}_3$, with an applied field of 1000 Oe under the FC conditions (200–5 K).

remains at around 130 K for all systems, consistent with the resistivity results.

D. Calculations and analysis

We want to understand two main effects seen in our experiments. First, the ground state changes upon hole doping, and second, the T_c does not change. To understand these features, we considered several ferromagnetic and AFM configurations: FM- (a, b, c) , AFM- c , and FM-canted. Here, (a, b, c) denote the crystal axes along which the magnetic moments can point. In the FM-canted configuration, the magnetic moments are canted $\sim 18^\circ$ from the b axis. Out of these AFM- c and FM-canted are seen in experiment, along with FM- b . We also considered FM- a and FM- c to check if we find the right easy-axis for the ground state in our calculations.

We carried out DFT calculations using the Elk code [39], including spin-orbit coupling via the second variational formulation. We used the Perdew-Burke-Ernzerhof (PBE) form of the exchange-correlation functional [40], with a basis cutoff RG_{max} of 8.0 and a k -point grid of $4 \times 8 \times 8$. Fermi surfaces were plotted using XCrySDen [41]. We note that treatment of disorder in this framework, including spin-orbit coupling is computationally prohibitively expensive.

The density of states (DOS) for experimentally observed magnetic configurations, FM- b , AFM- c , and FM-canted, are shown in Fig. 4. In all cases, the predominant contribution at the Fermi level comes from Cr states. The main effect of doping is a shift of ~ 0.08 eV for most of the features in the DOS for these magnetic configurations. The magnetic moment for both undoped and doped systems is close to $2\mu_B$ in the different studied FM configurations. For the FM- b configuration, the magnetic moment reduces from 2.07 to $2.01\mu_B$ upon doping, while for FM-canted configuration, it decreases from 2.11 to $1.98\mu_B$. We also show in Fig. 5 the evolution of Fermi surfaces with doping. Different colors represent different bands crossing the Fermi level. For the

two FM configurations, the main effect of hole doping is to enlarge the central hole pocket, shown in yellow, which has significant Cr contribution. By estimating the change in volume of this hole pocket, we found the change in hole density to be $\sim 0.7 \times 10^{22} \text{ cm}^{-3}$, which is the same order of magnitude value as the experimental estimate.

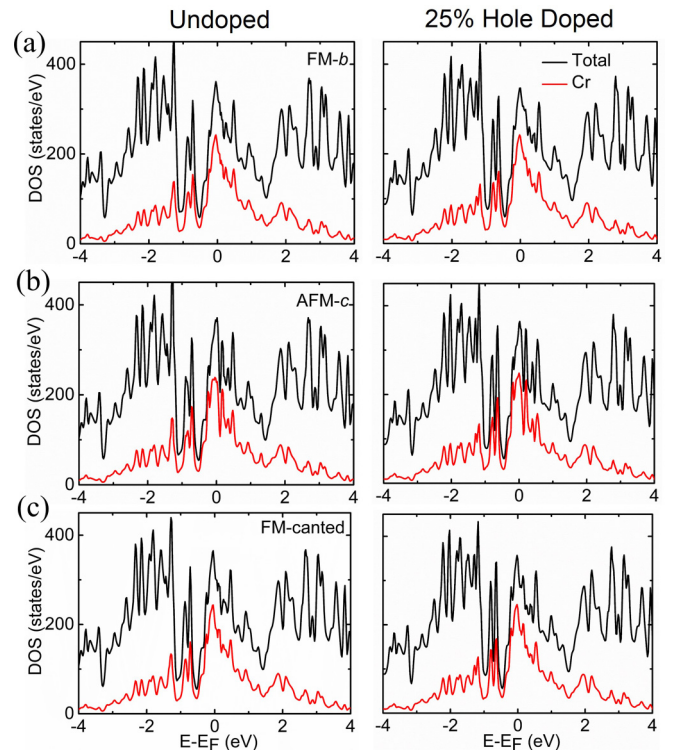


FIG. 4. DOS for (a) FM- b , (b) AFM- c , and (c) FM-canted magnetic configurations for undoped (left panel) and 25% hole doped systems (right panel).

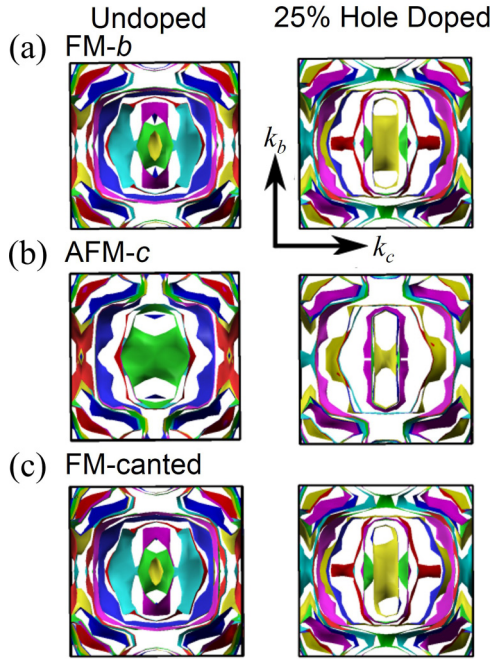


FIG. 5. Fermi surfaces for (a) FM- b , (b) AFM- c , and (c) FM-canted magnetic configurations for undoped (left panel) and 25% hole doped systems (right panel).

Table II contains a summary of the energies of different magnetic configurations. If one were to estimate the energy scale of exchange coupling from these energies, it would result in a T_c smaller than that experimentally observed. This could either be due to errors in the PBE functional, which can underestimate magnetic energy differences [42] or could be due to the Heisenberg model not providing an appropriate description of this system. Within DFT-PBE, we always find that the FM- b magnetic ordering is lowest in energy, although for the undoped case, the experimental configuration FM-canted is very close in energy by 0.22 meV. On hole doping, the FM-canted configuration becomes less stable, i.e., it becomes higher in energy compared to FM- b , reproducing the trend seen in our experiments. The Sb atoms contribute substantially to the spin-orbit energy, and we find that upon doping, the occupation of Sb atoms changes by about 0.25 electrons per unit cell. This change in occupation may, therefore, tip over the fine balance between the relative stability of FM-canted and FM- b magnetic configurations. This is a likely reason why we can control the relative energy of the two FM configurations using doping.

To summarize, from our first-principles calculations, we find results that are qualitatively in agreement with experiments, in that (i) the canted order becomes less stable with doping, (ii) FM- b is the most stable FM structure, and (iii) the magnetic moment is similar to the experimental

TABLE II. Energy for different magnetic configurations. The energy of the ferromagnetic state with the spins pointing along the b axis is chosen as the reference. Ferromagnetic arrangement with spins pointing along the a axis (FM- a), along the c axis (FM- c), antiferromagnetic arrangement along the c axis (AFM- c), and a ferromagnetic configuration with spins canted from the b axis (FM-canted) are considered.

Magnetic configuration	Energy undoped (meV)	Energy 25% hole doped (meV)
FM- a	1.25	3.16
FM- b	0	0
FM- c	0.54	2.17
FM-canted	0.22	1.43
AFM- c	2.19	3.17

value for both doped and undoped compounds. Overall, the calculations support our experimental interpretation that the introduction of holes into the system can control the magnetic ordering in LaCrSb₃, potentially via changing the occupation of the Sb atoms.

III. CONCLUSION

To tune and control the complex FM and AFM orders in LaCrSb₃, doping in the La site was designed and successfully realized. Our studies demonstrate that hole doping in the highly anisotropic magnetic material LaCrSb₃ can effectively suppress the AFM spin canting order and transform the magnetic complexity into simply a FM lattice. Our first-principles DFT calculations show that the canted magnetic order becomes energetically less favorable compared to the FM order upon hole doping. Our studies reveal an effective mean to tune competing orders in LaCrSb₃.

ACKNOWLEDGMENTS

This paper was supported by the Center for Emergent Superconductivity, an Energy Frontier Research Center funded by the U.S. Department of Energy, Office of Science, Office of Basic Energy Sciences, under Award No. DEAC0298CH1088. Computational resources were provided by the University of Illinois Campus Cluster. We made use of the Electron Probe Instrumentation Center (EPIC) facility of the Northwestern University Atomic and Nanoscale Characterization Experimental Center (NUANCE) Center at Northwestern University, which has received support from the Soft and Hybrid Nanotechnology Experimental (SHyNE) Resource (NSF NNCI-1542205), the Materials Research Science and Engineering Center (MRSEC) program (NSF DMR-1121262) at the Materials Research Center, the International Institute for Nanotechnology (IIN), the Keck Foundation, and the State of Illinois through the IIN.

- [1] J. G. Bednorz and K. A. Müller, *Z. Phys. B* **64**, 189 (1986).
 [2] C. Petrovic, P. G. Pagliuso, M. F. Hundley, R. Movshovich, J. L. Sarrao, J. D. Thompson, Z. Fisk, and P. Monthoux, *J. Phys.: Condens. Matter* **13**, L337 (2001).

- [3] Y. Kamihara, T. Watanabe, M. Hirano, and H. Hosono, *J. Am. Chem. Soc.* **130**, 3296 (2008).
 [4] M. N. Baibich, J. M. Broto, A. Fert, F. Nguyen Van Dau, F. Petroff, P. Etienne, G. Creuzet, A. Friederich, and J. Chazelas, *Phys. Rev. Lett.* **61**, 2472 (1988).

- [5] J. G. Bednorz and K. A. Müller, *Phys. Rev. Lett.* **52**, 2289 (1984).
- [6] S. Park and T. R. Shroud, *J. Appl. Phys.* **82**, 1804 (1997).
- [7] J. H. Haeni, P. Irvin, W. Chang, R. Uecker, P. Reiche, Y. L. Li, S. Choudhury, W. Tian, M. E. Hawley, B. Craigo, A. K. Tagantsev, X. Q. Pan, S. K. Streiffer, L. Q. Chen, S. W. Kirchoefer, J. Levy, and D. G. Schlom, *Nature (London)* **430**, 758 (2004).
- [8] H. Takahashi, K. Igawa, K. Arii, Y. Kamihara, M. Hirano, and H. Hosono, *Nature (London)* **453**, 376 (2008).
- [9] X. H. Chen, T. Wu, G. Wu, R. H. Liu, H. Chen, and D. F. Fang, *Nature (London)* **453**, 761 (2008).
- [10] M. Rotter, M. Tegel, and D. Johrendt, *Phys. Rev. Lett.* **101**, 107006 (2008).
- [11] F. Steglich, J. Aarts, C. D. Bredl, W. Lieke, D. Meschede, W. Franz, and H. Schäfer, *Phys. Rev. Lett.* **43**, 1892 (1979).
- [12] S. Friedemann, T. Westerkamp, M. Brando, N. Oeschler, S. Wirth, P. Gegenwart, C. Krellner, C. Geibel, and F. Steglich, *Nat. Phys.* **5**, 465 (2009).
- [13] E. Schubert, M. Tippmann, L. Steinke, S. Lausberg, A. Steppke, M. Brando, C. Krellner, C. Geibel, R. Yu, Q. M. Si, and F. Steglich, *Science* **351**, 485 (2016).
- [14] R. M. Kusters, J. Singleton, D. A. Keen, R. McGreevy, and W. Hayes, *Phys. B (Amsterdam, Neth.)* **155**, 362 (1989).
- [15] K. I. Chahara, T. Ohno, M. Kasai, and Y. Kozono, *Appl. Phys. Lett.* **63**, 1990 (1993).
- [16] X. Zhang, J. Li, B. Foran, S. Lee, H. Y. Guo, T. Hogan, C. R. Kannewurf, and M. G. Kanatzidis, *J. Am. Chem. Soc.* **117**, 10513 (1995).
- [17] V. Brouet, W. L. Yang, X. J. Zhou, Z. Hussain, N. Ru, K. Y. Shin, I. R. Fisher, and Z. X. Shen, *Phys. Rev. Lett.* **93**, 126405 (2004).
- [18] K. Y. Shin, V. Brouet, N. Ru, Z. X. Shen, and I. R. Fisher, *Phys. Rev. B* **72**, 085132 (2005).
- [19] C. Malliakas, S. J. L. Billinge, H. J. Kim, and M. G. Kanatzidis, *J. Am. Chem. Soc.* **127**, 6510 (2005).
- [20] H. J. Kim, C. D. Malliakas, A. T. Tomic, S. H. Tessmer, M. G. Kanatzidis, and S. J. L. Billinge, *Phys. Rev. Lett.* **96**, 226401 (2006).
- [21] M. A. Zhuravleva, M. Evain, V. Petricek, and M. G. Kanatzidis, *J. Am. Chem. Soc.* **129**, 3082 (2007).
- [22] C. D. Malliakas and M. G. Kanatzidis, *J. Am. Chem. Soc.* **131**, 6896 (2009).
- [23] H. M. Eiter, M. Lavagnini, R. Hackl, E. A. Nowadnick, A. F. Kemper, T. P. Devereaux, J. H. Chu, J. G. Analytis, I. R. Fisher, and L. Degiorgi, *Proc. Natl. Acad. Sci. USA* **110**, 64 (2013).
- [24] M. J. Ferguson, R. W. Hushagen, and A. Mar, *J. Alloys Compd.* **249**, 191 (1997).
- [25] M. L. Leonard, I. S. Dubenko, and N. Ali, *J. Alloys Compd.* **303-304**, 265 (2000).
- [26] L. Deakin, M. J. Ferguson, A. Mar, J. E. Greedan, and A. S. Wills, *Chem. Mater.* **13**, 1407 (2001).
- [27] L. Deakin and A. Mar, *Chem. Mater.* **15**, 3343 (2003).
- [28] S. J. Crerar, L. Deakin, and A. Mar, *Chem. Mater.* **17**, 2780 (2005).
- [29] D. D. Jackson and Z. Fisk, *Phys. Rev. B* **73**, 024421 (2006).
- [30] M. Inamdar, A. Thamizhavel, and S. Ramakrishnan, *J. Magn. Magn. Mater.* **320**, 2766 (2008).
- [31] N. Raju, J. E. Greedan, M. J. Ferguson, and A. Mar, *Chem. Mater.* **10**, 3630 (1998).
- [32] I. S. Dubenko, P. Hill, and N. Ali, *J. Appl. Phys.* **89**, 7326 (2001).
- [33] D. D. Jackson, M. Torelli, and Z. Fisk, *Phys. Rev. B* **65**, 014421 (2001).
- [34] E. Granado, H. Martinho, M. S. Sercheli, P. G. Pagliuso, D. D. Jackson, M. Torelli, J. W. Lynn, C. Rettori, Z. Fisk, and S. B. Oseroff, *Phys. Rev. Lett.* **89**, 107204 (2002).
- [35] X. Lin, V. Taufour, S. L. Bud'ko, and P. C. Canfield, *Philos. Mag.* **94**, 1277 (2014).
- [36] See Supplemental Material at <http://link.aps.org/supplemental/10.1103/PhysRevB.94.134411> for details of the experimental details, energy dispersive spectrum, resistivity analysis, Hall resistivity, magnetization at small magnetic field, and structure refinements of compounds with other doping levels.
- [37] N. Rivier and A. E. Mensah, *Phys. B+C (Amsterdam)* **91**, 85 (1977).
- [38] T. Hoang and D. Jackson, APS March Meeting, March 21–25, Los Angeles, CA, <http://meetings.aps.org/link/BAPS.2005.MAR.V9.13> (2005).
- [39] The Elk FP-LAPW code, <http://elk.sourceforge.net/> (accessed August 08, 2016).
- [40] J. P. Perdew, K. Burke, and M. Ernzerhof, *Phys. Rev. Lett.* **77**, 3865 (1996).
- [41] A. Kokalj, *Comp. Mater. Sci.*, **28**, 155 (2003).
- [42] B. Busemeyer, M. Dagrada, S. Sorella, M. Casula, and L. K. Wagner, *Phys. Rev. B* **94**, 035108 (2016).